Reweighted Sparse- Least-Mean Mixed-Norm Adaptive Control for Solar PV Integrated EV Charging Station

Anjeet Verma, *Member, IEEE and* Bhim Singh, *Fellow, IEEE*
Indian Institute of Technology, New Delhi, India
anjeet15@gmail.com

***Abstract*— Connecting a large number of electric vehicle (EV) to the distribution system, causes the unbalanced loading of the three phases and thereby resulting in the excessive neutral current to flow in the neutral wire of the transformer. To address these issues, in this paper, a solar photovoltaic (PV) array powered multifunctional EV charging station is proposed. The charging station provides the facility to connect multiple single phase EV chargers. Moreover, the charging station employs a voltage source converter (VSC) to interface the PV array and storage battery. The VSC of the charging station performs the multiple tasks such as, (1) extraction of maximum power of the PV array, (2) compensation of neutral current, (3) compensation of harmonics current and reactive power requirement of the EVs, (4) making the three phase source currents balanced and sinusoidal, (5) improvement in the power quality of source voltage and current, and (6) dynamic power management. To achieve all these functionalities, the VSC of the charging station, is controlled using the reweighted sparse least mean mixed norm (RS-LMMN) based adaptive control algorithm. The proposed control algorithm utilizes the benefits of both LMS, and LMF based adaptive control algorithm on minimizing the steady-state error, and improving the convergence rate. Moreover, the proposed control algorithm also adds the correction factor for sparsity in the input matrix. This further improves the tracking capability, convergence rate, and reduces the steady state error. The prototype of the charging station, is used to validate the control algorithm and the various claimed functionalities experimentally.**

***Keywords*— Electric Vehicle, Charging Station, SPV Generation, Multifunctional VSC, Power Quality.**

I. INTRODUCTION

Since last decade, the automotive industry is undergoing a paradigm shift from conventional internal combustion engine based vehicle to the electric vehicle (EV). As a result, more than two million people are already using EVs by the end of 2016 [1]. Since the electric energy is the spine of the EVs, many residential and public charging stations are installed. Most of the EVs are charged using the single-phase onboard charger [2]. However, connecting a large number of EVs with different power level, creates an unequal loading of the three phase of the grid. Because of this, huge harmonics current flows through the secondary winding of the transformer. Moreover, a large neutral current also flows through the neutral wire of the transformer. This may lead to the bursting of the neutral conductor [3]. Therefore, in this paper, a charging station is proposed that provides the facility to connect the single phase charger while keeping the neutral current zero even with the unequal loading of the three phases of the supply system.

Another paradigm shift, the world is undergoing through, is the generation of electricity from the renewable energy sources [4]. Following it, the proposed charging station, integrates the photovoltaic (PV) array for charging the EVs. Verma et al. [5], Abeywardana et al. [6], and Yan et al. [7] have suggested the PV array integrated EV charger for self-sustained, reliable, clean and cost-effective charging. Choudhari et al. [8] have proposed the SPV integrated smart charging for PHEV, in which a DC-DC boost converter is utilized to interface the PV array and the charger. Monteiro et al. [9] have also integrated the PV array to EV charger using a DC-DC boost converter. However, in this paper, the DC-DC conversion stage is eliminated, and the PV array is directly interfaced to the charging station using a diode.

Various publications have been reported the control the PV array assisted charging station. Tazay et al. [10] have discussed the d-q theory based control of the hybrid converter for an EV charging station. However, the control algorithm uses the phase locked loop (PLL), and the dq-to-abc transformation, which requires a lot of computation. Moreover, the control does not consider the nonlinearity of the EV charger. Because of it, the charger injects the harmonics into the grid. Therefore, in the present work, RS-LMMN based control algorithm is used, that takes the nonlinearity of the EV chargers into account.

Out of various adaptive filters discussed in the literatures [11], the least mean squares (LMS) based adaptive filter is used widely owing to its simple structure, and easy implementation. However, the convergence speed of LMS algorithm has strong dependency on the eigenvalue distribution of the input-signal autocorrelation matrix. Another disadvantage of the LMS algorithm is that, it utilizes fixed step size for updating the filter adaptation coefficients, which requires the tradeoff between the convergence speed and maladjustment error [12]. Moreover, the LMS algorithm [13] exhibits some stability issue due to appearance of some undamped response as the sampling time increases. Another famous adaptive algorithm is the recursive least squares (RLS) algorithm [14]. The RLS algorithm utilizes the best

978-1-5386-6625-8/18/$31.00

approximation of Wiener solution to find the least square error at each iteration based on all the previous data. Due to it, the RLS algorithm converges quickly. However, the RLS algorithm is computationally expensive, and numerically unstable for ill input conditions.

The data-reusing LMS (DR-LMS) algorithm [15] utilizes the received signal and current desired signal several times in each iteration to converge quickly. The performance can be enhanced using normalized and unnormalized new data-reusing LMS (NNDR-LMS and UNDR-LMS) where the past data is also used in each iteration along with the current desired output and the current input [16].

In this paper, RS-LMMN based adaptive control algorithm is used for implementation of PV array integrated multiport multifunctional charging station. The proposed control algorithm utilizes the features of both LMS and LMF algorithm for performance improvement. The RS-LMMN algorithm also uses a penalty factor for the sparsity of input signal matrix to improve the convergence speed.

II. System Description

The proposed charging station is designed to charge the electric vehicles using single phase onboard charger in three phase four wire configuration of the distribution system as shown in Fig. 1. Each EV is connected between the phase, and the neutral wire. A four leg VSC is coupled to the point of common coupling (PCC) of charging station using a coupling inductor. A PV array is interfaced to the DC bus (DCB) of the charging station through a diode. This diode stops the reverse power flow from DCB to the PV array. A storage battery connected at charging station using a DC-DC converter ensures the uninterruptible charging operation of the charging station under energy deficit condition. A RC ripple filter is utilized to eliminate the high-frequency noise caused by the switching of VSC.

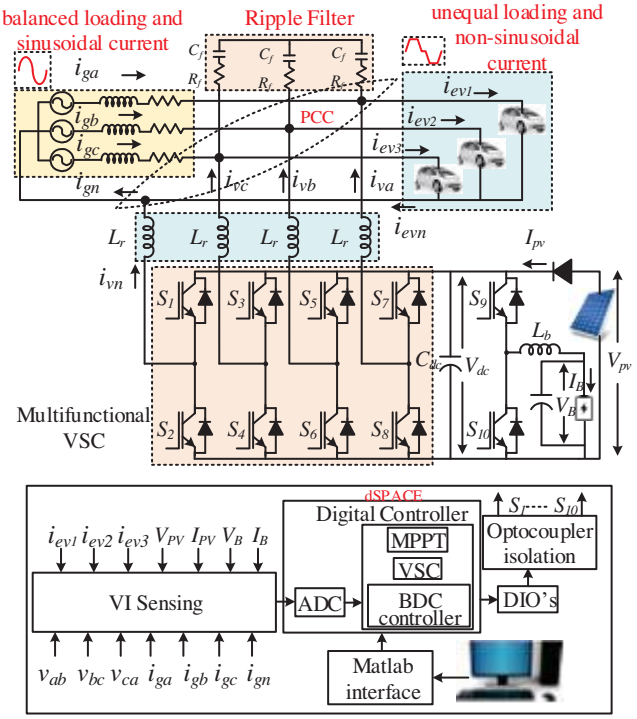

Fig. 1 Circuit diagram of proposed charging station

III. Control Algorithm

The proposed charging station is designed to charge the multiple EVs simultaneously using the SPV array power. Therefore, the control algorithm aims to utilize the PV array power maximally without much disturbing the grid. The control algorithm is designed to perform the following tasks.

- Estimation of maximum power point (MPP) voltage of the SPV array, and regulation of the DC link voltage equal to the MPP voltage for maximum power extraction.
- Control the flow of PV array power through VSC to the EVs for charging.
- Control the power exchange with the source depending upon the EV charging requirement, storage battery requirement and PV generation.
- Ensure the unity power factor operation (UPF) of the source. This means that no harmonics current or reactive power exchange with the source. Moreover, make the source currents balanced and sinusoidal all the time, even the different loading of the three phases.
- The zero neutral current to flow into the source.
- Manage the power flow balance among different components of the charging station even under transient condition.
- Control the charging/discharging current of the storage battery.

Based on these tasks, the control of the charging station is divided into the subsections such as (1) MPPT and DCB voltage control, (2) Control of multifunctional VSC, and (3) control of bi-directional DC-DC converter.

A. MPPT and DC Bus Voltage Control

In the proposed charging station, VSC harnesses the maximum possible power of the PV array by regulating the DCB voltage (V_{dc}) to such a value at which the impedance seen by the PV array equals the internal impedance of PV array itself. However, the voltage corresponding to the maximum power (V_{dc}^*) is estimated using the maximum power point tracking (MPPT) algorithm. An incremental conductance (INC) [17] based MPPT algorithm is used here. However, in case of unavailable PV power generation, the DCB voltage (V_{dc}^*) is regulated at fixed value of 400V. A proportional integral (PI) controller is utilized to maintain the DCB voltage equal to the reference DCB voltage (V_{dc}^*). The mathematical formulation of PI controller response (I_d) is given as,

$$I_d(s) = I_d(s-1) + k_{pd}\{V_{de}(s) - V_{de}(s-1)\} + k_{id}V_{de}(s) \quad (1)$$

Where V_{de} is the voltage error and k_{pd}, k_{id} are the gains of the PI controller.

B. Control of Multifunctional VSC

The control diagram of VSC is exhibited in Fig. 2. The purpose of the VSC control algorithm is to estimate the active (I_p) and a reactive component (I_q) of the charging current. For it, the RS-LMMN based adaptive control algorithm is used. Using I_p , I_q currents, the reference sinusoidal source currents (i_{ga}^*, i_{gb}^*, i_{gc}^*) are obtained, and the gate pulses of the VSC are generated. The detail description of the control algorithm is discussed as follows.

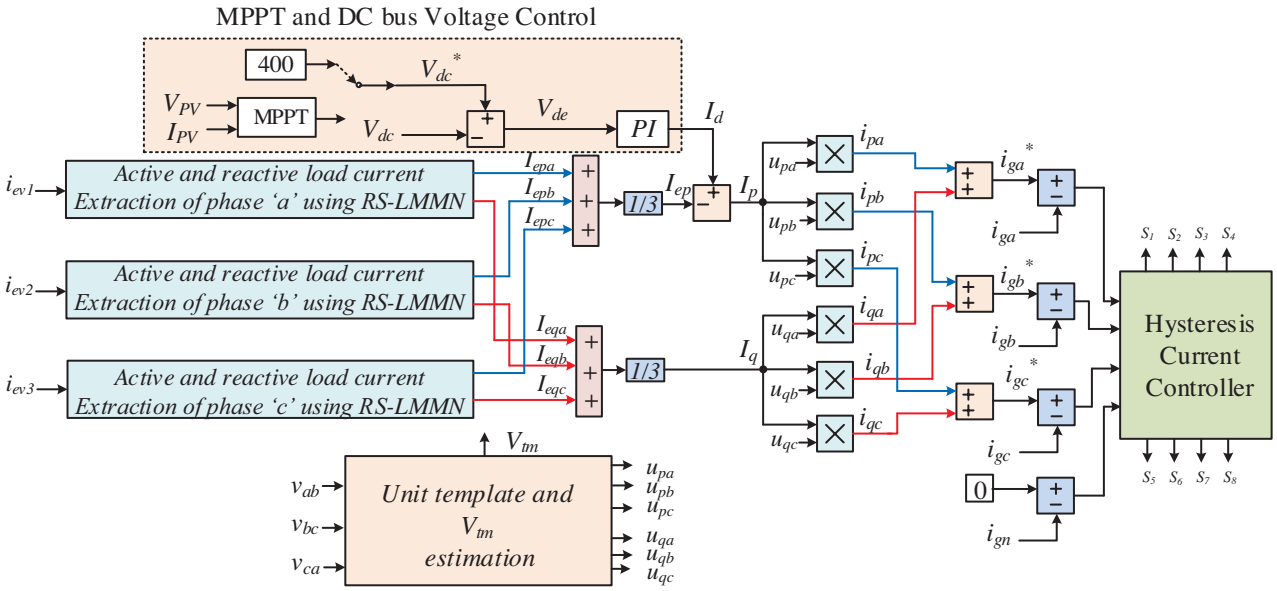

Fig. 2 Control algorithm schematic

1) Estimation of PCC Voltage Amplitude, In-phase and Quadrature-phase Unit Templates

The amplitude of the PCC voltage amplitude is estimated as [3].

$$V_{tm} = \sqrt{\frac{2}{3}} \times \sqrt{v_{ga}^2 + v_{gb}^2 + v_{gc}^2} \tag{2}$$

Where, v_{ga}, v_{gb}, and v_{gc} are the phase to neutral voltage of the source. The phase to neutral voltages are calculated using the line voltages (v_{ab} and v_{bc}) at PCC as,

$$v_{ga} = \frac{1}{3}\left(2v_{ab} + v_{bc}\right), v_{gb} = \frac{1}{3}\left(-v_{ab} + v_{bc}\right), v_{gc} = \frac{1}{3}\left(-v_{ab} - 2v_{bc}\right) \tag{3}$$

The in-phase unit (u_{pa}, u_{pb}, u_{pc}) and quadrature phase (u_{qa}, u_{qb}, u_{qc}) unit templates are estimated as,

$$u_{pa} = \frac{v_{ga}}{V_{tm}}, u_{pb} = \frac{v_{gb}}{V_{tm}}, u_{pc} = \frac{v_{gc}}{V_{tm}} \tag{4}$$

$$u_{qa} = -\frac{u_{pa}}{\sqrt{3}} + \frac{u_{pc}}{\sqrt{3}}, u_{qb} = \frac{\sqrt{3}u_{pa}}{2} + \frac{(u_{pb} - u_{pc})}{2\sqrt{3}} \tag{5}$$

$$u_{qc} = -\frac{\sqrt{3}u_{pa}}{2} + \frac{(u_{pb} - u_{pc})}{2\sqrt{3}}$$

2) Estimation of Weight of Real Component of Desired Source Currents

The weight of real component of charging current for phase 'a' (I_{epa}) is estimated as,

$$I_{epa}(r+1) = \underbrace{I_{epa}(r) + me_a(r)\left\{d + (1-d)e_a^2(r)\right\}u_{pa}(r)}_{LMMN\ algorithm} - r\underbrace{\frac{\mathrm{sgn}\left[I_{epa}(r)\right]}{1 + z\left|I_{epa}(r)\right|}}_{Sparse\ penalty} \tag{6}$$

Where, μ is the step-size, $\rho = \mu\gamma\zeta$, is regularization factor, which decides the level of trade-off between the estimation error and sparsity strength. ζ controls reweighting factor, and its value is defined as $\zeta<0$, whereas γ value is defined as $\gamma>0$. δ is the constant, which decides the nature of the adaptive algorithm, and it is defined as $0 \le \delta \le 1$. For $\delta=1$, the LMMN algorithm poses the feature of LMS. However, for $\delta=0$, the LMMN algorithm behaves as LMF algorithm. Therefore, δ value is selected between 0 and 1 to take the benefits of both the LMS and LMF algorithms. The schematic of RS-LMMN [18] algorithm is shown in Fig. 3.

The sgn[I_{epa}] is the component-wise function, which is defined as,

$$\mathrm{sgn}\left[I_{epa}\right] = \begin{cases} \dfrac{I_{epa}}{\left|I_{epa}\right|} & I_{epa} \neq 0 \\ 0 & I_{epa} = 0 \end{cases} \tag{7}$$

The addition of the sparse penalty speeds up the convergence of the proposed RS-LMMN based control algorithm.

Similarly, the real weights component of charging current for phase 'b' and 'c', are estimated as,

$$I_{epb}(r+1) = I_{epb}(r) + \mu e_b(r)\left\{\delta + (1-\delta)e_b^2(r)\right\}u_{pb}(r) - \rho\frac{\mathrm{sgn}\left[I_{epb}(r)\right]}{1 + \zeta\left|I_{epb}(r)\right|} \tag{8}$$

$$I_{epc}(r+1) = I_{epc}(r) + \mu e_c(r)\left\{\delta + (1-\delta)e_c^2(r)\right\}u_{pc}(r) - \rho\frac{\mathrm{sgn}\left[I_{epc}(r)\right]}{1 + \zeta\left|I_{epc}(r)\right|} \tag{9}$$

Using (6), (8), and (9) the total weight of the real components of the charging current, is obtained as,

$$I_{ep} = \frac{I_{epa} + I_{epb} + I_{epc}}{3} \tag{10}$$

The total weight of the real component of the desired source current, is obtained as,

$$I_p = I_d - I_{ep} \tag{11}$$

3) Estimation of Weight of Reactive Component of Desired Source Currents

Using (6), the weight of reactive components (I_{eqa}, I_{eqb}, and I_{eqc}) of charging currents, are given as,

$$I_{eqa}(r+1) = I_{eqa}(r) + \mu e_a(r)\left\{\delta + (1-\delta)e_a^2(r)\right\}u_{qa}(r) - \rho\frac{\mathrm{sgn}\left[I_{eqa}(r)\right]}{1 + \zeta\left|I_{eqa}(r)\right|} \tag{12}$$

$$I_{eqb}(r+1) = \underbrace{I_{eqb}(r) + \mu e_b(r)\left\{\delta + (1-\delta)e_b^{\,2}(r)\right\}u_{qb}(r)}_{LMMN\ algorithm} - \underbrace{\rho \frac{\mathrm{sgn}\left[I_{eqb}(r)\right]}{1+\zeta\left|I_{eqb}(r)\right|}}_{Sparse\ penalty} \quad (13)$$

$$I_{eqc}(r+1) = I_{eqc}(r) + \mu e_c(r)\left\{\delta + (1-\delta)e_c^{\,2}(r)\right\}u_{qc}(r) - \rho \frac{\mathrm{sgn}\left[I_{eqc}(r)\right]}{1+\zeta\left|I_{eqc}(r)\right|} \quad (14)$$

The total weight of the reactive component of the desired source current, is obtained as,

$$I_q = \frac{I_{eqa} + I_{eqb} + I_{eqc}}{3} \quad (15)$$

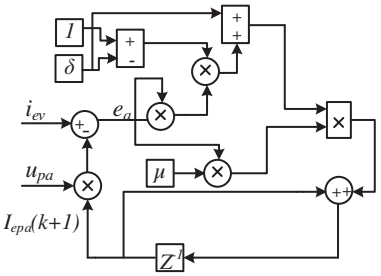

Fig. 3 Schematic of RS-LMMN algorithm

4) Estimation of Sinusoidal Desired Source Currents

Using (11) and (15), the sinusoidal desired real (i_{pa}, i_{pb}, i_{pc}) and sinusoidal desired reactive (i_{qa}, i_{qb}, i_{qc}) source currents, are estimated as,

$$i_{pa} = I_p \times u_{pa}, i_{pb} = I_p \times u_{pb}, i_{pc} = I_p \times u_{pc} \quad (16)$$

$$i_{qa} = I_q \times u_{qa}, i_{qb} = I_q \times u_{qb}, i_{qc} = I_q \times u_{qc} \quad (17)$$

Finally, using (16) and (17), the desired source currents (i_{ga}^*, i_{gb}^*, i_{gc}^*) are obtained as,

$$i_{ga}^* = i_{pa} + i_{qa}, i_{gb}^* = i_{pb} + i_{qb}, i_{gc}^* = i_{pc} + i_{qc} \quad (18)$$

The VSC gate pulses are generated through the hysteresis current controller.

C. Bi-directional DC-DC Converter Control

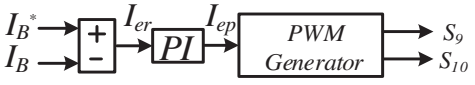

Fig. 4 DC-DC converter control

The control of the storage battery connected at DCB using a bi-directional DC-DC converter is given in Fig. 4. The EV charges/discharges at constant current. Based on the charging/discharging, the desired current can be positive or negative. The expression of PI controller for constant current mode is given as,

$$I_{ep}(k) = I_{ep}(k-1) + k_{ep}\{I_{er}(k) - I_{er}(k-1)\} + k_{ei}I_{er}(k) \quad (19)$$

Where I_{er} is the error, and k_{ep} and k_{ei} are proportional and integral gains of the PI controller. Now the gating pulses are generated using the PWM generator.

IV. Results And Discussion

The experimental performance of the proposed charging station, and its control algorithm under steady state condition and dynamic state condition, are shown in Figs. 5-9. A PV array of 5.6kW is used in the implementation of the charging station. The PV array is emulated using the Ametek TerraSAS SPV emulator. The open circuit voltage and short circuit current of the PV array, are 460V and 15A, respectively. However, the maximum power point (MPP) voltage and current of the PV array, are 396V and 14.2A, respectively. Since the EV chargers draw the non-sinusoidal current from the source, a diode bridge rectifier followed by the resistive-inductive load is used to emulate the EV charger. The insulated gate bipolar junction transistors (IGBTs) are used to design the multifunction VSC and the DC-DC converter for a storage battery. A 240V, 35Ah lead acid battery is used as a storage battery. The 5Ω resistor and 10μF electrolytic capacitor are used to design the ripple filter. Various Hall Effect based voltage (LEM make LV-25) and current sensor (LEM make LA-55) are used for sensing the system parameters. The sensed voltage and current signals are converted into a digital signal using analog to digital converters. Using these digital signals, the control algorithm of the charging station is implemented in the digital controller (dSPACE 1006), and the control signals are generated for VSC, and DC-DC converter.

A. Steady State Performance

The steady state performance of the charging station when the charging station is fully powered by the solar PV array, and three EVs, and a storage battery are charged using the PV power, is exhibited in Fig. 5. The excess power is also supplied to the source at a unity power factor (UPF) as justified by the unity displacement power factor (DPF) in Figs. 5 (j)-(o). The PV array is generating 5.6 kW of electrical energy as given in Fig. 5(a). Out of the 5.6kW, 2.77kW (EV1+EV2+EV3=0.93kW+0.89kW+0.95kW) is consumed by the three EVs, the storage battery takes 550W, and remaining 2.21kW power (phase 'a'+phase 'b' +phase 'c'= 0.73kW+0.75kW+0.73kW=2.21kW) is fed back to the source at UPF. Figs. 5 (b)-(g) show the voltages (v_{ga}, v_{gb},v_{gc}), currents (i_{ev1}, i_{ev2}, i_{ev3}), and power of the EVs. Figs. 5 (h)-(i) show the voltage (V_B), current (I_B) and power of the storage battery. Similarly, Figs. 5 (j)-(o) show the per phase voltages (v_{ga}, v_{gb},v_{gc}), currents (i_{ga}, i_{gb}, i_{gc}), and power of the source. While supplying power to the source, the total harmonic distortion (THD) of the source line voltage (v_{ab}) and line current (i_{ga}) is also observed at 1.8% and 4.3%, respectively as shown in Fig. 5 (p)-(q). Whereas, the THD of the current drawn by the EV1 (i_{ev1}) is 28% as shown in Fig. 5(r). Since the EVs connected at charging station, draw the unequal and non-sinusoidal current, the neutral current (i_{evn}) is significant as shown in Fig. 5(s) However, the source neutral current (i_{gn}) is almost reduced to very small value (Fig. 5(t)) because the VSC of the charging station, is supplying the neutral current (i_{vn}) as in Fig. 5(u). Moreover, the unbalanced phase currents are also mitigated by the VSC. Due to it, the source currents become balanced and sinusoidal.

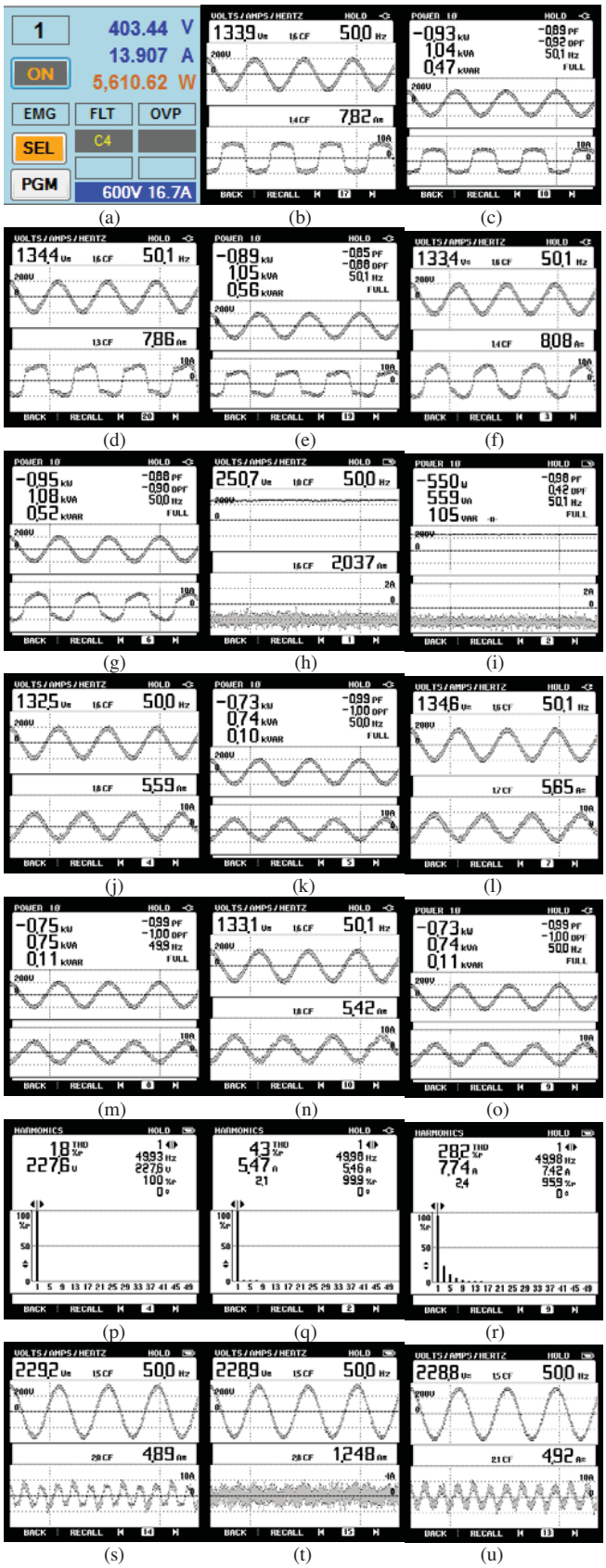

Fig. 5 Steady state performance, (a) V_{pv}, I_{pv}, and power, (b)-(c) v_{ga}, i_{ev1}, and EV1 power, (d)-(e) v_{gb}, i_{ev3}, and EV2 power, (f)-(g) v_{gc}, i_{ev3}, and EV3 power, (h)-(i) V_b, I_b, and power, (j)-(k) v_{ga}, i_{ga}, and power, (l)-(m) v_{gb}, i_{gb}, and power, (n)-(o) v_{gc}, i_{gc}, and power, (p) harmonic spectra of v_{ab}, (q) harmonic spectra of i_{ga}, (r) harmonic spectra of harmonic spectra of i_{ev1}, (s) i_{evn}, (t) i_{gn}, (u)i_{vn}

B. Dynamic Performance

During the operation, the charging station undergoes the transient caused by the change in solar irradiance, connection/disconnection of the EVs, and a change in the storage battery charging/discharging. The performance under these transients, is shown in Figs. 6-8.

1) Performance Under Solar Irradiance Change

Since the solar irradiance changes throughout the day, therefore, the controller of the charging station should be fast enough to observe the solar irradiance change, and it should be able to harness the maximum power under all irradiance condition. Moreover, the charging of the other EVs should not be affected, and the power equilibrium in the system should not be affected. Usually, the solar irradiance changes gradually, however, in this implementation, the worst case is considered, and the solar irradiance is changed in step from 1000W/m^2-400W/m^2. Due to change in the solar irradiance, the PV generated power reduces as the PV current reduces as shown in Figs. 6(a)-(b). Since the PV power is inadequate to meet the charging demand of the EVs, the charging station starts drawing power from the source. On the contrary, the power is being fed into the source before the change in solar irradiance change. The charging of the EV and charging of the storage battery, do not get affected by the solar irradiance change.

2) Performance Under Connection/Disconnection of EVs and Change in Charging Current of Storage Battery

Throughout the day, the EVs are connected/disconnected at the charging station, and their charging currents change dynamically. Under this condition, the charging of the other EVs should not be affected, and power equilibrium should be achieved. Figs. 7(a)-(c) show the performance under a sudden disconnection of EV1. Due to disconnection of the EV1, the power required for charging the EVs reduces. As a result, the power supplied to the source increases since the PV generation is not affected by these transients. The disconnection of EV1 does not affect the charging of other EVs as shown in Fig. 7 (b). Moreover, to balance the power, the source phase 'a' current increases as shown in Fig. 7(b). The disconnection does not affect the source's neutral current, and it remains zero. Moreover, after the disconnection of the EV1, the VSC current becomes equal to the source phase 'a' current. Fig. 7(d) shows the performance of the charging station when the storage battery is changed from charging to discharging.

3) Multifunctional Operation of VSC

Figs. 8 (a)-(b) exhibit the performance of the charging station with or without VSC in operation. From Fig. 8(a), it is understood that without VSC in operation, the source current is not sinusoidal because the harmonics current required by the EVs are being drawn from the source. Moreover, due to unbalanced charging, the neutral current is also significant. After switching 'ON' VSC, the source current becomes sinusoidal and neutral current also becomes zero as VSC is supplying the harmonics current and the neutral current. From Fig. 8 (b) it is observed that the VSC neutral current is equal to the neutral current caused by the EVs. Fig. 8(b) also exhibits that the performance of the VSC under disconnection of EV1. Fig. 8(c) exhibits the voltage correction capability of VSC under distorted source voltage condition. After switching 'ON' VSC, the source voltage becomes sinusoidal.

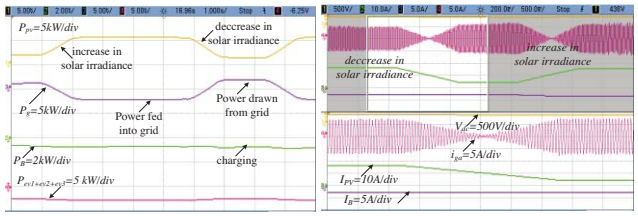

(a) (b)

Fig. 6 Dynamic performance under solar irradiance change

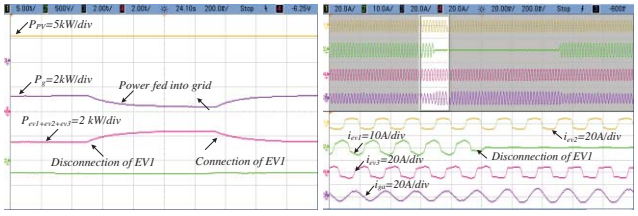

(a) (b)

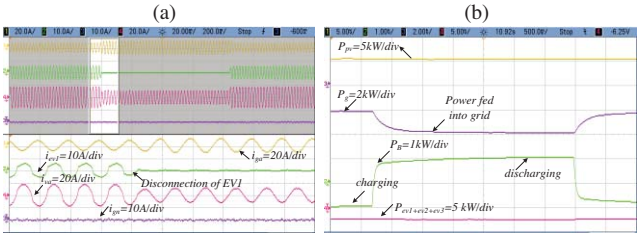

(c) (d)

Fig. 7 Dynamic performance under connection/disconnection of EVs, and change in charging/discharging current of storage battery

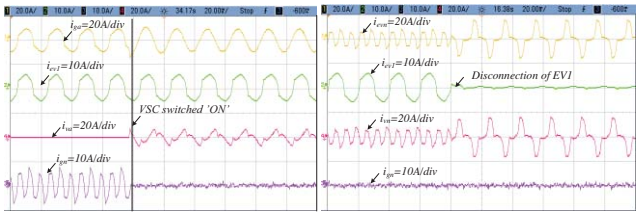

(a) (b)

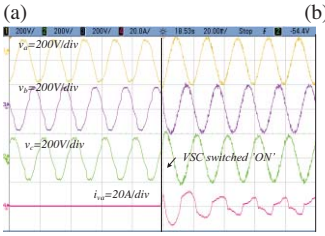

(c)

Fig. 8 Multifunctional operation of VSC, (a) neutral current compensation, (b) under EV connection/disconnection, (c) voltage correction capability

V. Conclusion

The experimental validation of a PV array powered multifunctional charging station and RS-LMMN based adaptive control algorithm, has been presented in this work. The presented results show that the three EVs multiple EVs can be charged simultaneously at the charging station with zero neutral current in the fourth wire of the distribution system at the unbalanced and nonlinear load. Moreover, the three phase's source currents are also maintained balanced and sinusoidal. While charging the EVs, the power quality of the source voltage and current, is also improved, and the THD is always maintained less than 5% as required by the IEEE 519 standard. The removal of the DC-DC converter power stage of the PV array has not affected the performance of the charging station, and presented results show that the maximum PV power is extracted under all operating conditions. The presented results have also verified the controller ability to manage the power flow balance under different transients caused by the solar irradiance change, EVs connection and disconnection and change in charging/discharging current of the storage battery. The comprehensive evaluation of the presented results have proved the competency of the proposed topology and its control algorithm for the development of charging station.

Acknowledgement

The authors are very grateful to the Renew Power Ventures Pvt. Ltd. for funding this project under Grant Number: RP03461 (Charging Station for Electric Vehicles).

Appendices

SPV array: V_{oc}=460V, I_{sc}=15A, V_{MPP}=396V, I_{MPP}=14.2A
Source Supply: Three phase 230V (L-L RMS), 50Hz
Storage Battery: 240V 35Ah Lead Acid

References

[1] International Energy Agency-Global EV Outlook 2017-Two Million and Counting. [Online].Available: https://www.iea.org/publications/freepublications/publication/GlobalEVOutlook2017.pdf

[2] International Energy Agency-World Energy Outlook 2017. [Online]. Available: https://www.iea.org/weo2017/

[3] Bhim Singh, Ambrish Chandra and Kamal Al-Haddad, Power Quality: Problems and Mitigation Techniques. John Wiley & Sons, 2015.

[4] National Renewable Energy Agency- Distributed Solar Photo Voltaics For Electric Vehicle Charging [Online]. Available: https://www.nrel.gov/docs/fy14osti/62366.pdf

[5] A. Verma and B. Singh, "Multi-objective reconfigurable three phase off-board charger for EV," *in IEEE Transport. Electrificat. Conf. (ITEC-India)*, Pune, 2017, pp. 1-6.

[6] D. B. Wickramasinghe Abeywardana, P. Acuna, B. Hredzak, R. P. Aguilera and V. G. Agelidis, "Single-Phase Boost Inverter-Based Electric Vehicle Charger With Integrated Vehicle to Grid Reactive Power Compensation," *IEEE Trans. Power Electron.*, vol. 33, no. 4, pp. 3462-3471, 2018.

[7] Q. Yan, B. Zhang and M. Kezunovic, "Optimized Operational Cost Reduction for an EV Charging Station Integrated with Battery Energy Storage and PV generation," *IEEE Trans. Smart Grid*, Early Access.

[8] K. Chaudhari, A. Ukil, K. N. Kumar, U. Manandhar and S. K. Kollimalla, "Hybrid Optimization for Economic Deployment of ESS in PV-Integrated EV Charging Stations," *IEEE Trans. Ind. Informat*, vol. 14, no. 1, pp. 106-116, Jan. 2018.

[9] V. Monteiro, J. G. Pinto and J. L. Afonso, "Experimental Validation of a Three-Port Integrated Topology to Interface Electric Vehicles and Renewables With the Electrical Grid," *IEEE Trans. Ind. Informat.*, vol. 14, no. 6, pp. 2364-2374, June 2018.

[10] A. Tazay and Z. Miao, "Control of a Three-Phase Hybrid Converter for a PV Charging Station," *IEEE Trans. Energy Convers.*, Early Access.

[11] Ali H. Sayed, Robust *Adaptive Filters*, 1, Wiley-IEEE Press, 2008.

[12] B. Widrow; J.M. McCool; M. Larimore and C.R. Johnson; "Stationary and non-stationary learning characteristics of the LMS adaptive filter;" in *Proc. of IEEE*, Vol. 64, no. 8, pp. 1151-1162, Aug. 1976.

[13] N. Beniwal, I. Hussain and B. Singh, "Implementation of DSTATCOM with i-PNLMS Based Control Algorithm under Abnormal Grid Conditions," *IEEE Trans. Ind. App.*, Early Access.

[14] M. Han, S. Zhang, M. Xu, T. Qiu and N. Wang, "Multivariate Chaotic Time Series Online Prediction Based on Improved Kernel Recursive Least Squares Algorithm," *IEEE Trans. Cybernetics*, Early Access.

[15] A. Rathore and D. K. Panda, "Performance analysis of data reusing least mean square algorithm for smart antenna system," *in IEEE Int. Conf. Comput., Communicat. and Automat.,* 2017, pp. 1391-1394.

[16] M. T. H. Alouane, "A square root normalized LMS algorithm for adaptive identification with non-stationary inputs," in *J. of Communicat. and Netw.*, vol. 9, no. 1, pp. 18-27, March 2007.

[17] J. Liu, J. Li, J. Wu and W. Zhou, "Global MPPT algorithm with coordinated control of PSO and INC for rooftop PV array," in *The J. of Eng.*, vol. 2017, no. 13, pp. 778-782, 2017.

[18] Y. Li, Y. Wang and F. Albu, "Sparse channel estimation based on a reweighted least-mean mixed-norm adaptive filter algorithm," *24th Euro. Sig. Process. Conf.,* 2016, pp. 2380-2384.